



Feature-preserving ultrasound speckle reduction via L_0 minimization

Lei Zhu^{a,b}, Weiming Wang^c, Xiaomeng Li^a, Qiong Wang^{c,*}, Jing Qin^b, Kin-Hong Wong^a, Kup-Sze Choi^b, Chi-Wing Fu^a, Pheng-Ann Heng^{a,c}

^a Department of Computer Science and Engineering, The Chinese University of Hong Kong, China

^b School of Nursing, The Hong Kong Polytechnic University, China

^c Shenzhen Key Laboratory of Virtual Reality and Human Interaction Technology Shenzhen Institutes of Advanced Technology, Chinese Academy of Sciences, China

ARTICLE INFO

Article history:

Received 23 January 2017

Revised 26 September 2017

Accepted 5 March 2018

Available online 12 March 2018

Communicated by Dr Bo Du

Keywords:

Ultrasound speckle reduction

L_0 minimization

GAP

Half-quadratic splitting method Iteratively re-weighted least squares framework

ABSTRACT

Speckle reduction is a crucial prerequisite of many computer-aided ultrasound diagnosis and treatment systems. However, most existing speckle reduction filters tend to concentrate the blurring near the features and introduce the hole artifacts, making the subsequent processing procedures complicated. Optimization-based methods can globally distribute such blurring, leading to better feature preservation. Motivated by this, we propose a novel optimization framework based on L_0 minimization for feature preserving ultrasound speckle reduction. We present an observation that the GAP, which integrates gradient and phase information, is extremely sparser in despeckled images (output) than in speckled images (input). Based on this observation, we propose an L_0 minimization framework to remove speckle noise and simultaneously preserve features in the ultrasound images. It seeks for the L_0 sparsity of the GAP values, and such sparsity is achieved by reducing small GAP values to zero in an iterative manner. Since features have larger GAP magnitudes than speckle noise, the proposed L_0 minimization is capable of effectively suppressing the speckle noise. Meanwhile, the rest of GAP values corresponding to prominent features are kept unchanged, leading to better preservation of those features. In addition, we propose an efficient and robust numerical scheme to transform the original intractable L_0 minimization into several sub-optimizations, from which we can quickly find their closed-form solutions. Experiments on synthetic and clinical ultrasound images demonstrate that our approach outperforms other state-of-the-art despeckling methods in terms of noise removal and feature preservation.

© 2018 Elsevier B.V. All rights reserved.

1. Introduction

Ultrasonography has become one of the most favorable imaging modalities in a wide range of clinical applications because it is safe, real-time and cost effective. However, ultrasound images are usually corrupted with granular patterns of white and dark spots that are referred as speckle [1]. Although speckle is sometimes considered as diagnostic clues on certain occasions, it has adverse effects on precise diagnosis and treatment in most cases [2]. In addition, speckle complicates automatic processing and analysis procedures of ultrasound images [3], including detection, segmentation, registration, and so on. Therefore, speckle reduction is a crucial prerequisite of many intelligent ultrasound systems [4].

Many ultrasound speckle reduction methods have been proposed. These methods can be roughly classified into two groups: wavelet-based filters [5] and spatial filters [2,6,7]. Assuming that the multiplicative speckle noise can be transformed into additive Gaussian noise by the logarithm operation, Wavelet-based methods decomposed the content of the transformed image into multiple sub-bands at different orientations and resolution scales. Although those methods can effectively remove speckle noise, they tended to produce the ringing artifacts when preserving features [8]. By exploiting the spatial correlation, spatial filters computed a despeckling result as a weighted average on a set of candidates. According to the candidate selection, those filters are divided into the local filters [6,9] and nonlocal filters [7]. However, spatial filters would concentrate the blurring near edges and introduced the hole artifacts [10]. In order to overcome such limitation, the optimization-based approaches have been proposed with state-of-the-art results in many image processing tasks [11]. Those methods globally distributed such blurring in spatial filters

* Corresponding author.

E-mail address: wangqiong@siat.ac.cn (Q. Wang).

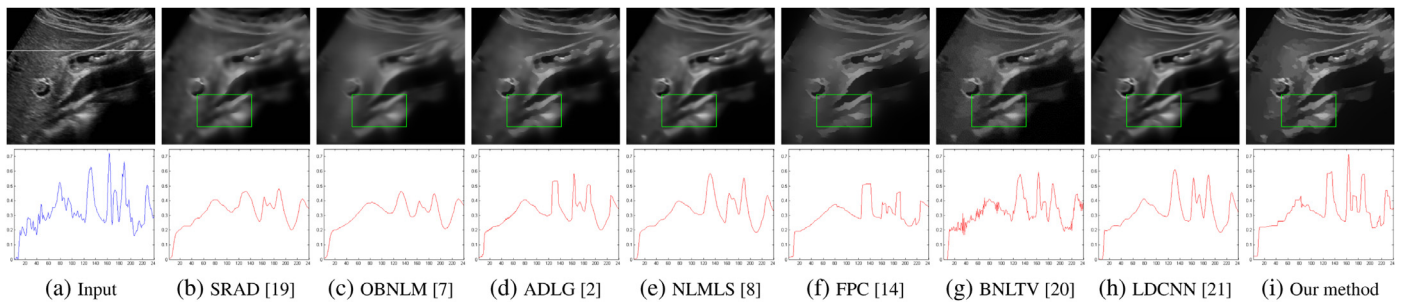


Fig. 1. Comparison of speckle reduction on an ultrasound image with gallstones, and the evaluation of the feature contrast preservation. (a) Original image with the intensity profile (blue curve) in a horizontal line. Despeckled result with its intensity profile (red curve) by (b) SRAD [19], (c) OBNLM [7], (d) ADLG [2], (e) NLMLS [8], (f) FPC [14], (g) BNLTv [20], (h) LDCNN [21], and (i) our method (For interpretation of the references to color in this figure legend, the reader is referred to the web version of this article.).

into each pixel [12], causing excellent restored results without hole artifacts. In addition, the spatial filters cannot preserve sharp edges like the global optimization based filters [12]. Recently, a global optimization based despeckling method, which assigns different penalties for speckle noise and features in a weighted-least-squares filter manner [13], is proposed in [14]. However, in order to suppress speckle noise, salient edges unavoidably received some penalties, leading to reduce feature contrasts and blur features in some degrees. To circumvent this problem, Xu et al. [11] proposed a L_0 norm based optimization to globally control how many non-zero entries are maintained using progressively thresholding procedures, and thus non-zero salient edges can be better preserved. Unfortunately, directly employing existing L_0 minimization [11,15–17] cannot achieve satisfactory results for speckle reduction, since the gradient information is inefficient to differentiate features from speckle noise in ultrasound images [18].

In this paper, we proposed a novel global optimization based on an L_0 minimization framework for feature-preserving speckle reduction in ultrasound images. Motivated by the sparseness prior of the image gradient and the feature detection capability of the local phase based feature asymmetry (FA) operator [22], we defined a new measurement (namely GAP) combining the gradient and the FA operators together. The GAP inherits those two properties. Consequently, we proposed a L_0 GAP minimization for speckle reduction in ultrasound image. It seeks for the L_0 sparsity of the GAP by progressively reducing low GAP values, which correspond to the speckle noise, to zero. Meanwhile, the significant features with high GAP values are kept unchanged. The proposed approach also has better performance in preserving low contrast features than existing despeckling methods, due to the intensity invariant property of the phase-based operator (FA) for feature detection. In addition, we proposed an efficient solver to minimize the proposed L_0 regularized objective function. A variable splitting strategy is employed to transfer the original optimization into the iterative optimization of a non-linear quadratic optimization and a L_0 regularized least square with a hard thresholding closed-form solution. For the non-linear quadratic optimization, the nonlinear FA measurement is linearized, producing a series of pure quadratic minimizations, for which an efficient and robust solution exists. Fig. 1 compares the despeckling performance of different methods. As shown in the top row, the proposed approach effectively preserves the boundaries of important features while other methods tend to blur the edges in different degrees (see the green rectangle). The advantages of our approach can be further verified by carefully checking the intensity profile of a horizontal line in the bottom row. When smoothing out the intensity fluctuations caused by speckle noise, existing methods also remove or largely reduce the intensity peaks at some features. In contrast, our approach hardly alters the intensity values of those peaks so that the features are almost totally retained in the despeckled image.

The contributions of this paper can be summarized as:

- We present a sparsity prior in the ultrasound image based on the observation that the GAP values in the despeckled image is highly sparser than that in the speckled image.
- We propose a L_0 norm regularized global optimization framework to seek for the GAP sparsity. During the pursuit of the sparsity, the proposed L_0 minimization can eliminate speckle noise in ultrasound images and better preserve features than previous despeckling techniques.
- We propose an efficient and robust solver to minimize the proposed objective function by first splitting the intractable problem into tractable sub-problems with half-quadratic splitting method, followed by the decomposition of the non-convex sub-problem into linear systems using iteratively re-weighted least squares.

This work extends its conference version [23] with differences as follows: (1) We refine the optimization procedure of our numerical solution in Section 3.3, where we present how we devise the solution (shown in Eq. 11) of a non-linear term regularized quadratic optimization (see Eq. 9) using the iterative re-weighted least squares (IRLS) framework, as well as the solution (see Eq. 15) of the L_0 regularized least squares (see Eq. 12) in the Appendix section. (2) We provide more validations (including comparisons with four recent despeckling works [8,14,20,21]), more comparisons on new clinical images, and more results of our method on new clinical images. (3) We add a new application in Section 4.5 by comparing the lesion boundary preservation of different despeckled results, as shown in Fig. 15. From the results, we can find that our despeckled result has smallest MRD (see Eq. (20) for its definition) value among all the MRD results, which implies that the despeckling method has a better edge preservation after speckle reduction, compared to other despeckling techniques. We will release our code upon the publication of this work.

The remainder of this paper is organized as follows. We first review some related works in Section 2. After that, details of our approach are described in Section 3, and Section 4 presents many experimental results on both synthetic and clinical ultrasound images, and two applications about the segmentation and the tumor boundary preservation. Finally, we conclude the paper and discuss some future work in Section 5.

2. Related work

Many despeckling methods have been proposed in the literature, and they can be categorized into two classes. The first one is the wavelet-based filters, which assumed that multiplicative speckle noise can be transformed into the additive Gaussian noise by the logarithm operation. After the logarithm transformation, the image content was decomposed into multiple. Large coefficients corresponded to the important low frequency information (e.g.,

edges), and noise and image details lied in the high frequency sub-bands. Usually, thresholding techniques were applied to the small coefficients for noise removal. Khare et al. [24] detected strong edges using the imaginary part of the complex scaling coefficients and then performed the shrinkage on the magnitude of complex wavelet coefficients at non-edge pixels. The threshold value of the shrinkage was determined by the statistical parameters of complex wavelet coefficients of the noised image. Recently, Esakkirajan et al. [5] proposed an adaptive wavelet packet domain filtering for speckle reduction. They produced a rich set of bases with the wavelet packet decomposition technique and then the singular value decomposition was used to select the best basis. The modified NeighShrink thresholding technique was executed on all other sub-bands, except the sub-band with the largest singular value. Wavelet-based despeckling techniques can effectively preserve texture details, but they tend to produce ringing artifacts when preserving features [8].

Another direction for speckle reduction in ultrasound images is the spatial filters. Those methods compute a despeckling output by utilizing the spatial correlation existing in images. One is to extend the nonlinear anisotropic diffusion filtering (ADF) [25] for the ultrasound data corrupted with speckle noise. They [2,19,26] encouraged the isotropic diffusion in the homogeneous regions for noise removal, while stop the diffusion between homogeneous regions for feature preservation. Yu and Acton [19] proposed the speckle reducing anisotropic diffusion (SRAD) by involving the edge-sensitive instantaneous coefficient of variation to determine whether a pixel should be smoothed or left intact in the ultrasound image. Zhang et al. [27] employed the Laplacian pyramid to decompose the image into different sub-bands and then applied anisotropic diffusion with different diffusion fluxes to suppress the noise in each sub-band layer. Yu et al. [18] devised a diffusion framework by using the Smallest Univalued Segment Assimilating Nucleus (SUSAN) operator to act as the edge detector. Recently, Flores et al. [2] proposed a ADF based despeckling method for the breast ultrasound image, where the conduction coefficient parameter involved in the ADF was adaptively selected for each pixel under the guidance of the 2D Log-Gabor filter response. Even though these diffusion based despeckling techniques can progressively smooth the speckled image, a lot of meaningful details are also discarded.

Another spatial filter group is to estimate the despeckled result of each pixel by weighted averaging on pixels in a local region or the entire image. Early investigations focus on adaptive filters, e.g., Kuan filter [28]. Those despeckling methods evaluated the variation degree inside the filtering window, so that regions with the low coefficient of variation were smoothed by the low-pass filtering for eliminating speckle noise, while regions with the high variation coefficient were with the identity filtering for protecting features. Tay et al. [9] proposed the squeeze box filter (SBF) based upon removing outliers with a local extremum. By replacing these outliers with the local mean in each iteration, the SBF method compressed the image pixel values, so that the differences in interclass means were protected for feature preservation, while the interclass variance was reduced for speckle noise removal. Balocco et al. [6] proposed an automatic bilateral filter dedicated for the ultrasound images by embedding the noise statistics into the weighting scheme of the original bilateral filter framework. Taking the assumption that there are many repetitive patches in the image, the non-local means (NLM) method [29] averaged all pixels in the entire image, and the weights were computed by the weighted Euclidean distance between two patches. This strategy leads to a more robust denoising performance when compared to local filters. However, the original NLM was designed for suppressing the additive Gaussian noise in 2D natural images, and thus several despeckling techniques were proposed to adapt the NLM

method for the multiplicative speckle noise model in ultrasound images. Couple et al. [7] utilized the Bayesian theory to define a Pearson distance for patch comparisons and implemented the NLM method in the block-wise manner to decrease the computational burden. Recently, Yang et al. [8] combined local statistics of the ultrasound image and NLM filter to reduce speckle in ultrasound images. However, when there are not enough similar patches within the ultrasound image, those methods tend to produce severe artifacts and the performance degrades significantly.

Recently, many attractions in the image processing domain has transformed from the spatial filters to the global optimization [10,11,13], which usually consisted of a data term and regularization terms. Compared to the spatial filters, global optimization outperformed in the sharp feature preservation [12]. In addition, spatial filters would concentrate the blurring near these edges and introduce the holes while the global optimization based methods would globally distribute such blurring to each pixel of the image. Although a recent study [14] formulated a global method for speckle reduction, but it tend to penalize the salient edges. Recently, an advanced optimization framework, called L_0 minimization, is presented by globally counting the number of non-zero entries to approximate the underlying signal in a sparsity-control manner, and thus salient structures with large entry values are allowed in the output image, causing better preservation of those important edges. Unfortunately, existing L_0 minimization models [11,15–17] employed the pixel intensity difference (e.g., gradient information) to seek for the sparsity. When applying those methods for despeckling, speckle noise and features will receive similar penalties, since ultrasound speckle manifests itself as a form of multiplicative noise, which indicates that variances (including gradient magnitudes) caused by speckle noise are comparable or even larger than edges [18]. Note that several works developed the deep learning frameworks for additive Gaussian noise removal [21] or image classification [30], but those deep models are trained in a different noise distribution from the speckle noise in ultrasound images. Hence, those methods tend to blur features while eliminating speckle noise of ultrasound images; see Figs. 1, 3, 4, 6–10, 14, 15.

3. Methods

In this paper, we propose a L_0 minimization tailored for speckle reduction in ultrasound images. Specifically, we propose to seek for the sparsity of the term GAP (Sections 3.1 and 3.2), since it can effectively separate features and speckle noise in ultrasound images, and progressively reducing small GAP values to 0 by solving the L_0 minimization enables speckle noise to be suppressed. Moreover, we devise an efficient optimization procedure based on the half-quadratic splitting technique and the iteratively re-weighted least squares framework to solve the proposed L_0 minimization (Section 3.3).

3.1. Feature asymmetry

Local energy model developed in [31] postulates that features are perceived at points where the phase information is highly coherent. Based on this assumption, the features in the image can be located by analyzing the phase pattern of each pixel [32]. Inspired from this, Belaid et al. [22] presented a local phase-based operator, feature asymmetry (FA) [33], using Cauchy filters, to measure the significance of features in ultrasound images:

$$\begin{cases} FA = \frac{||R_0| - |R_e| - \Theta|}{\sqrt{R_0^2 + R_e^2 + \varepsilon_1}}, \\ R_0 = g * S, R_e = (g * z_1 * S, g * z_2 * S), \end{cases} \quad (1)$$

where Θ describes the estimated noise threshold and $[\cdot]$ is the zeroing operation of negative values; ε_1 is a constant to avoid

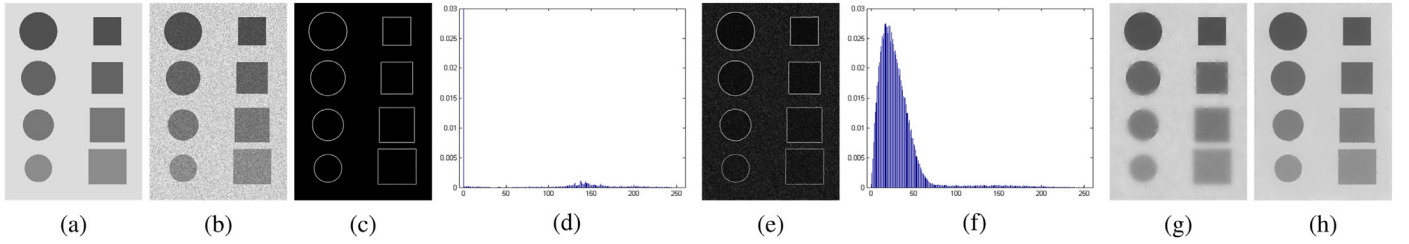


Fig. 2. Statistical analysis of GAP: (a) a clean image, (b) corresponding synthetic speckled image (noise variance $\sigma^2=0.08$), (c) GAP map of (a), (d) GAP magnitude histogram of (c), (e) GAP map of (b), (f) GAP magnitude histogram of (e). Despeckled result of (b) by L_0 gradient minimization [11] and (h) our method. Obviously, GAP is much sparser in the despeckled image, compared to the speckled image.

division by zero, and its value is set as 0.0001; z_1 and z_2 are the Riesz filters; g is the Cauchy filter. In the frequency domain, the definition of g [34] is given by:

$$G(\theta) = |\theta|^\varphi \exp(-t|\theta|) \sqrt{\frac{\pi 4^{\varphi+1} t^{2\varphi+1}}{\Gamma(2\varphi+1)}}, \quad (2)$$

where Γ is the gamma function; θ denotes the normalized coordinates of each pixel. φ and t are the bandwidth and the scaling parameter of the Cauchy kernel, respectively. The value of the FA measure ranges between 0 and 1, close to 0 in smooth regions and close to 1 near the features.

Note that the scale parameter t in the Cauchy kernel is important for the quality of edge detection. Generally, details and discontinuities are maintained in fine scales while coarse scales preserve the regularities and continuities of the boundaries. Hence, finding the optimal scale that fits to the features in the image is very crucial because a finer scale might include unwanted details while a coarser scale might miss important features. We employ the following γ normalized edge strength measure Ω_γ [14,35] for optimal scale selection:

$$\Omega_\gamma = -t^{3\gamma} (H_x^3 H_{xxx} + 3H_x^2 H_y H_{xxy} + 3H_x H_y^2 H_{xyy} + H_y^3 H_{yyy}). \quad (3)$$

Here, $\gamma = 0.5$, as suggested in [14,35], H is the filtered image obtained by convolving the input image with the Cauchy kernel at scale t ; $H_{(\cdot)}$ denotes the partial derivative operator. To determine the optimal scale, we analyze the intensity distribution of Ω_γ over all a scale range and then select the one where the sum of intensities achieves the maximal value.

3.2. The proposed L_0 minimization framework

Given an ultrasound image J , we define a new measurement, called GAP, by combining Gradient And Phase information:

$$GAP(J) = \partial_x J^2 + \partial_y J^2 + FA(J)^2, \quad (4)$$

where $\partial_x J^2$ and $\partial_y J^2$ are the gradient map at the x and y direction, respectively. $FA(J)$ denotes the feature map obtained by applying the local phase based feature asymmetry on J using Eq. (1). Basically, due to the combination of FA and gradient information, GAP can be considered as a feature detector in the ultrasound image, and it also has a sparse prior between the input ultrasound image and its despeckled one. Owing to these two properties, the GAP can guide our L_0 minimization to effectively remove speckle noise and simultaneously preserve underlying features which is achieved by progressively reducing smaller GAP values, which are corresponding to the speckle noise, to 0, while hardly altering larger GAP values corresponding to the features.

The proposed GAP can inherit characteristics of both the gradient information and the phase based FA, as shown in Fig. 2. First, GAP can be a good edge indicator in speckled images. Fig. 2 (b) is a synthetic speckled image generated from a clean image (Fig. 2 (a)) by employing a theoretical speckle noise model [7] on it. The GAP

map of Fig. 2 (b) is shown by Fig. 2 (e), in which the boundaries of different shape objects have larger GAP values than speckle noise. Second, it is well known that a clean image has a sparser gradient magnitude distribution than its corresponding speckled image. We find that the GAP magnitude also has such sparse prior. Fig. 2 (c) and (d) are the GAP map and GAP histogram of Fig. 2 (a), respectively. It is obvious that only pixels at edges have non-zero GAP values and we can observe apparent zero peaks in the GAP histogram distribution. In contrast, for the speckled image (Fig. 2 (b)), its GAP distribution (Fig. 2 (f)) cannot be modeled by narrow peaks.

Motivated by these two properties of the GAP, we propose a novel L_0 minimization for feature-preserving ultrasound speckle reduction:

$$\min_D \left\{ \sum_q (D_q - I_q)^2 + \lambda \cdot P(D) \right\}, \text{ where } P(D) = \#\{p \mid |GAP(D)_p| \neq 0\}. \quad (5)$$

Here, I is the input image and D is the despeckled image; q is the pixel coordinate; $\#\{\}$ is a counting operator, outputting the number of p that satisfies $|GAP(D)_p| \neq 0$; $P(D)$ is the L_0 norm of the GAP. It globally counts the number of pixels whose GAP values are non-zero in the image D . λ is a weight to control the significance of the GAP sparsity, and it in fact represents the noise removal ability of the proposed method. Fig. 2 (g) shows the despeckled result of Fig. 2 (b) via L_0 gradient minimization [11]. We can see that it over-smooths the shape boundaries in Fig. 2 (b), because the L_0 minimization with the gradient magnitude [11] could not distinguish features from the noise and smooth out many features during ultrasound speckle reduction. On the contrary, thanks to the better edge detection capability of the GAP, our method can effectively eliminate speckle noise and well protect shape boundaries simultaneously, as shown in Fig. 2 (h).

3.3. Numerical solution

Solving a L_0 norm regularized objective function is usually considered as computational intractable, because the first data term models the pixel-wise difference and the second regularization term represents a global L_0 metric [11]. We propose an efficient solver for our L_0 minimization based on the half-quadratic splitting method [36,37] and iteratively re-weighted least squares framework (IRLS) [38]. First, three auxiliary variables u , v and w are introduced to represent $\partial_x D$, $\partial_y D$ and FA , leading to a new energy function:

$$\min_{D,u,v,w} \left\{ \sum_q (D_q - I_q)^2 + \beta \left((\partial_x D_q - u_q)^2 + (\partial_y D_q - v_q)^2 \right) + (FA(D)_q - w_q)^2 + \lambda \cdot P(u, v, w) \right\}, \quad (6)$$

where q is the pixel index; $P(u, v, w) = \#\{p \mid u_p^2 + v_p^2 + w_p^2 \neq 0\}$; β controls the similarity between $(\partial_x D, \partial_y D, FA)$ and (u, v, w) , and

its value is increased by iteratively multiplying a constant value k . When $\beta \rightarrow \infty$, the solution of Eq. (6) converges to the one of Eq. (5). By initializing D as I , we minimize Eq. (6) for a given β by solving two tractable sub-problems to update D and those auxiliary variables (u, v, w) alternatively:

Sub-problem 1: Updating D . Given estimated values of (u, v, w) from previous iteration, we update D by solving:

$$\min_D \left\{ \sum_q (D_q - I_q)^2 + \beta \left((\partial_x D_q - u_q)^2 + (\partial_y D_q - v_q)^2 + (FA(D)_q - w_q)^2 \right) \right\}. \quad (7)$$

Unfortunately, due to the nonlinear property of $FA(D)$ (see Eq. (1)), the above quadratic optimization is still highly non-convex, and it is non-trivial to solve the minimization. Gradient descent methods require tens or hundreds of iterations, and the solution is sensitive to the initialization. Inspired by the iteratively re-weighted least squares framework (IRLS) [38], we propose a numerical solver to transform the highly non-convex optimization into solving a series of sparse linear equations, for which fast and robust solutions exist. The key idea is to decompose the nonlinear $FA(D)_q$ into a linear term D_q and a nonlinear term f_q by multiplying D_q at the numerator and denominator of $FA(D)_q$:

$$FA(D)_q \approx \frac{FA(D)_q}{D_q + \varepsilon_2} * D_q = f_q * D_q, \quad \text{where } f_q = \frac{FA(D)_q}{D_q + \varepsilon_2}, \quad (8)$$

where ε_2 is a small constant to avoid division by zero, and its value is empirically set as 0.0001. By incorporating f_q and D_q , we can re-formulate the minimization in Eq. (7) as:

$$\min_D \left\{ \sum_q (D_q - I_q)^2 + \beta \left((\partial_x D_q - u_q)^2 + (\partial_y D_q - v_q)^2 + (f_q D_q - w_q)^2 \right) \right\}. \quad (9)$$

Vector form. We re-write Eq. (9) using a vector form:

$$\min_{V_D} (V_D - V_I)^T (V_D - V_I) + \beta \left((C_x V_D - V_u)^T (C_x V_D - V_u) + (C_y V_D - V_v)^T (C_y V_D - V_v) + (F V_D - V_w)^T (F V_D - V_w) \right), \quad (10)$$

where V_D, V_I, V_u, V_v and V_w are the vector representation of $D, I, u, v,$ and w respectively; C_x and C_y are the Toeplitz matrices from the discrete gradient operators [39]; F is a diagonal matrix, and its i th diagonal element is: $F[i, i] = f_i$; Owing to the separation $FA(D)_q$ into the nonlinear f_q and the linear D_q , we can naturally obtain a numerically stable approximation by iteratively performing the following two steps, in a way similar to the iteratively re-weighted least squares (IRLS) optimization framework:

Step 1: Compute f_q with the estimated despeckled image D .

Step 2: Fixing f_q , we update D by solving the following sparse linear system:

$$(\Phi + \beta C_x^T C_x + \beta C_y^T C_y + \beta F^T F) V_D = V_I + \beta C_x^T V_u + \beta C_y^T V_v + \beta F^T V_w, \quad (11)$$

where Φ is the identity matrix with the same size of matrix C_x . We employ the preconditioned conjugate gradient (PCG) algorithm to solve the sparse linear equation, due to its linear computational complexity [39]. In our experiments, we find that 3 to 5 iterations of the IRLS optimization procedure are enough to estimate the despeckled image D .

Sub-problem 2: Updating (u, v, w) Given D , we estimate (u, v, w) by solving the following L_0 regularized least squares:

$$\min_{u, v, w} \left\{ \sum_q \left((\partial_x D_q - u_q)^2 + (\partial_y D_q - v_q)^2 + (FA(D)_q - w_q)^2 \right) + \frac{\lambda}{\beta} P(u, v, w) \right\}, \quad (12)$$

where $P(u, v, w)$ denotes the number of non-zero elements in the $(u^2 + v^2 + w^2)$. To minimize Eq. (12), we first re-formulate $P(u, v, w)$ as a sum of an element-wise term below:

$$P(u, v, w) = \# \left\{ a \mid u_a^2 + v_a^2 + w_a^2 \neq 0 \right\} = \sum_b R(u_b^2 + v_b^2 + w_b^2),$$

$$\text{where } R(u_b^2 + v_b^2 + w_b^2) = \begin{cases} 0, & u_b^2 + v_b^2 + w_b^2 = 0. \\ 1, & \text{otherwise.} \end{cases} \quad (13)$$

Thanks to the re-formulation, we can transform Eq. (12) into a new objective function, where each element u_q, v_q and w_q can be individually estimated:

$$\min_{u_q, v_q, w_q} \left\{ (\partial_x D_q - u_q)^2 + (\partial_y D_q - v_q)^2 + (FA(D)_q - w_q)^2 + \frac{\lambda}{\beta} R(u_q^2 + v_q^2 + w_q^2) \right\}. \quad (14)$$

Now, we can quickly obtain its closed-form solution of Eq. (14) under the condition below (see the APPENDIX A for the proof):

$$(u_q, v_q, w_q) = \begin{cases} (\partial_x D_q, \partial_y D_q, FA(D)_q), & GAP(D)_q > \frac{\lambda}{\beta}. \\ (0, 0, 0), & \text{otherwise.} \end{cases} \quad (15)$$

3.4. Why it works

Here, we provide more analysis on the proposed L_0 minimization. Algorithm 1 summarizes the whole optimization process. In

Algorithm 1 Ultrasound speckle reduction via L_0 minimization.

Require: The input ultrasound image I , smoothness λ , the bandwidth φ , scale range Ω , similarity parameters β_0, β_{max} and increasing rate k .

1: Initialization: $D^0 \leftarrow I, \beta = \beta_0$

2: **repeat**

3: with the estimated D , compute u, v, w using Eq. 15,

4: **for** $iter = 1$ to 5 **do**

5: **for all** scale $s \in \Omega$ **do**

6: compute FA using Eq. 1,

7: compute the edge strength Ω_γ using Eq. 3

8: **end for**

9: select the optimal scale with maximal Ω_γ value,

10: compute f_p with optimal scale using Eq. 8,

11: update D by solving the sparse linear equation (Eq. 11),

12: **end for**

13: $\beta = k\beta$

14: **until** $\beta \geq \beta_{max}$

15: **return** despeckled image D

our solver, we first introduce three auxiliary variables (u, v, w) and initialize them as: $(u, v, w) = (\partial_x D, \partial_y D, FA(D))$. Afterwards, two sub-problems are alternatively updated as following:

(a) For each pixel p of the current despeckled result D , we check whether $GAP(D)_p \leq \frac{\lambda}{\beta}$ is satisfied. If yes, we set $u_p = 0, v_p = 0,$ and $w_p = 0$, otherwise, the value is unchanged, as described in Eq. (15).

(b) We transfer the changes happened in (u, v, w) to $(\partial_x D, \partial_y D, FA(D))$ by solving Eq. (7), so that small values in the $GAP(D)$ are also largely reduced, or even set to 0. Meanwhile, the remaining $GAP(D)$ values are unaltered.

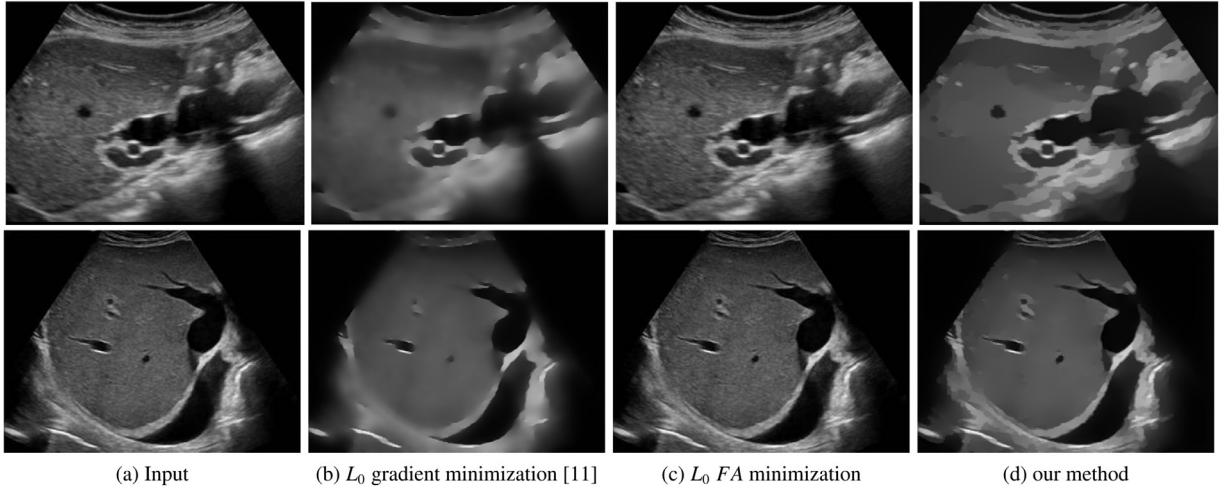


Fig. 3. Comparison of speckle reduction on an ultrasound image using different L_0 model. (a) Original image. Despeckled result produced by (b) L_0 gradient minimization [11], (c) L_0 FA minimization, and (d) our method.

When small $GAP(D)$ are progressively reduced to 0, their $\partial_x D$, $\partial_y D$ and $FA(D)$ values also become 0, leading to the decrease of $P(D)$. Hence, our solver can gradually minimize the proposed L_0 minimization. Once there is no pixel whose GAP value is below $\frac{\lambda}{\beta}$ in the current despeckled result D , our method reaches the convergence state. Similar to [17], our method with three auxiliary splitting variables also converges after 10–20 iterations. Since features have larger GAP values than speckle noise, $\partial_x D$ and $\partial_y D$ of speckle noise tend to be 0 as the iteration number increases, leading to the removal of speckle noise. At the same time, the values of $(\partial_x D, \partial_y D, FA(D))$ at features are almost unchanged, so that our method can well protect features. Furthermore, our method is also capable to preserve low contrast features, since FA is invariant to changes of brightness or contrast for feature detection.

Noted that using only L_0 gradient and only L_0 FA minimization cannot achieve satisfied result for ultrasound speckle reduction. Since gradient information is unable to separate features from speckle noise in ultrasound images, the L_0 gradient minimization [11] gives similar penalties on features and speckle noise, leading to feature blurring (see Fig. 3 (b)). Although FA has the capability to distinguish speckle noise and features, L_0 FA minimization also cannot effectively remove speckle noise. The reason is that setting the FA values of the speckle noise to 0 cannot alter the intensity value of the noise. Hence, the noise cannot be eliminated (see Fig. 3 (c)). In Fig. 3, we compare the despeckled results by the L_0 gradient minimization [11], L_0 FA minimization, and our method. As can be seen, L_0 gradient minimization removes many features, when suppressing the speckle noise in the ultrasound image, since those removed features have smaller gradient values than some speckle noise. The despeckled result by L_0 FA minimization is almost the same as the original ultrasound image. Owing to the advantages of GAP , our method can efficiently eliminate the speckle noise and preserve features, as shown in Fig. 3 (d).

4. Experiments

We evaluated the performance of the proposed method on many synthetic and clinical ultrasound images and compared its results with state-of-the-art despeckling methods: (1) speckle reducing anisotropic diffusion [19] (denoted as SRAD), (2) optimized Bayesian non-local means [7] (denoted as OBNLM), (3) anisotropic diffusion guided by Log-Gabor filters [2] (denoted as ADLG), (4) non-local mean filter combined with local statistics [8] (denoted as NLMLS), (5) fast feature-preserving speckle reduction via phase

congruency [14] (denoted as FPC), (6) nonlocal total-variation-based speckle filtering [20] (denoted as BNLTv), and (7) learning deep CNN Denoiser Prior [21] (denoted as LDCNN). To produce their results, we obtain their implementations from the public domain for SRAD, OBNLM, ADLG, and the authors for the FPC; for the NLMLS, we strictly follow the implementation details to implement it by ourselves; for BNLTv and LDCNN, we obtained the results directly from the authors. Moreover, we generate numerous results by exhaustively trying and fine-tuning many different parameters for all the compared methods, and select the best despeckled result for display.

Our method includes six parameters, namely, the smoothness λ , the bandwidth φ , the scale range Ω , the similarity parameters β_0 , β_{max} and the increasing rate k . In the all experiments, as suggested in [14,22], we set φ as 1.58; β_0 and β_{max} are empirically set as: $\beta_0 = 4\lambda$, $\beta_{max} = 1e5$, respectively, while the scale range Ω is empirically fixed as [1, 20]. The increasing rate k balances the time efficiency and despeckling performance, and its value is in the range of [1.2, 2]. λ is a critical parameter to adjust the performance of feature preservation, and we set its value in [1e–3, 1e–1] in all the experiments. A larger λ is required for an input image with a high noise level. Our Matlab implementation takes about 5 s to process a 300*255 ultrasound image.

4.1. Synthetic images

For the synthetic images, the ground truth images are available, and thus we can quantitatively evaluate and compare the performance of different despeckling methods by using three metrics: peak signal-to-noise ratio (PSNR) [40], Pratt's figure of merit (FOM) [19] and mean structural similarity (MSSIM) [41]. PSNR [40] describes the ratio between the ground truth image G and the despeckled image D :

$$PSNR = 10 \cdot \log_{10} \frac{M \cdot N}{\sum_{i=0}^{M-1} \sum_{j=0}^{N-1} [D(i, j) - G(i, j)]^2}, \quad (16)$$

where $[M, N]$ is the size of the despeckled image D . The higher PSNR is, the closer D is to the ground truth G . FOM [19] is used to compare the performance of edge preservation:

$$FOM = \frac{1}{\max\{E_D, E_G\}} \sum_{i=1}^{E_D} \frac{1}{1 + d_i^2 \rho}, \quad (17)$$

where E_D and E_G are the number of edge pixels in the despeckled output D and the ground truth G , respectively. The d_i is the

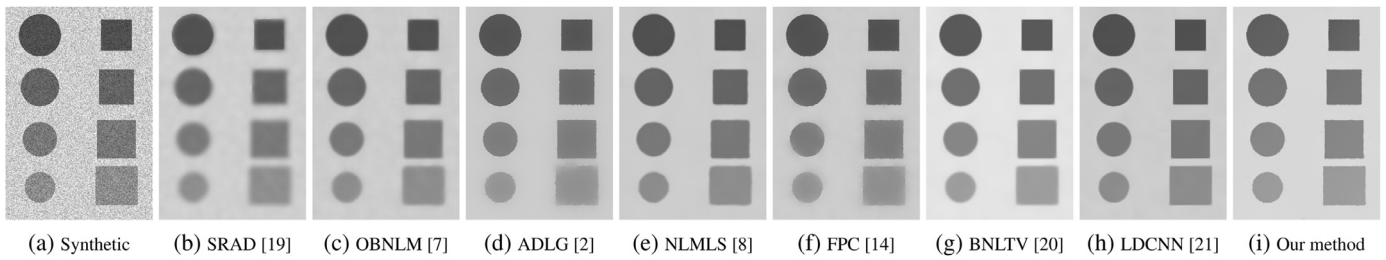


Fig. 4. (a) synthetic speckled image ($\sigma^2 = 0.15$). Despeckled result by (b) SRAD [19], (c) OBFLM [7], (d) ADLG [2], (e) NLMLS [8], (f) FPC [14], (g) BNLTv [20], (h) LDCNN [21], and (i) our method.

Table 1
Quantitative evaluation of different despeckled results.

	SRAD	OBFLM	ADLG	NLMLS	FPC	BNLTv	LDCNN	Ours
PSNR	22.85	23.54	23.61	24.44	23.72	26.33	25.22	27.09
FOM	0.3972	0.5126	0.5291	0.5739	0.5900	0.4730	0.6046	0.6333
MSSIM	0.8740	0.9155	0.9235	0.9484	0.9554	0.9576	0.9635	0.9729

Euclidean distance between the i th edge pixel in D and its nearest edge pixel in G . The ρ is a constant, and its value is usually set to be $1/9$. *FOM* takes value in $[0, 1]$, with unity for the best edge preservation.

MSSIM [41] adapts the human visual system to the structural information in a scene. It computes the image similarity between D and G by taking into account three measures: structure, contrast and luminance, and the formulation is

$$MSSIM(D, G) = \frac{1}{T} \sum_{i=1}^T SSIM((D)_i, (G)_i), \quad (18)$$

where T is the number of pixels in D and G , and *SSIM* is:

$$SSIM(D, G) = [S(D, G)]^{W_1} \times [C(D, G)]^{W_2} \times [L(D, G)]^{W_3}, \quad (19)$$

where $S(D, G)$, $C(D, G)$ and $L(D, G)$ are the luminance, contrast and structure similarity function, respectively. W_1 , W_2 and W_3 are their weights, and we set their values using the default one reported in [41]. The *MSSIM* value varies from 0 to 1, and a higher value indicates the less difference between D and G . The theoretical speckle noise model [7] is based on the equation: $Y = X + \Phi * X$, where X and Y are the noise-free and synthesized images with speckle noise, respectively, and Φ is the zero-mean Gaussian noise with variance σ^2 : $\Phi \sim \mathcal{N}(0, \sigma^2)$. We employed the above noise model on the clean image (Fig. 2(a)) to produce a synthetic speckled image (Fig. 4(a)) with noise variance $\sigma^2 = 0.15$. The clean image (Fig. 2 (a)) consists of shape objects with different sizes and intensity contrasts to the background. Fig. 4 (b)–(g) show despeckled results of different ultrasound speckle reduction algorithms. It is observed that all the other methods blur the shape boundaries to some extent, especially for the low contrast shapes in the last row. Thanks to the less sensitivity of phase information to intensity contrasts, the proposed approach achieves the best performance in preserving edges of all those shape objects while removing the speckle noise.

Table 1 reports quantitative values of all the three metrics among different despeckling methods. Clearly, our method achieves outperformed performance for all the three metrics (PSNR: 27.09, FOM: 0.6333, MSSIM: 0.9729), compared to other techniques. The higher *PSNR* value shows that our result is much closer to the ground truth for the pixel intensities. The largest *FOM* value indicates that our approach outperforms all the other methods on edge preservation. In the meantime, the superior performance with respect to the *MSSIM* value implies that our despeckled result is the most similar to the raw image in terms of structure, luminance and contrast. Furthermore, we test our

Table 2
Comparison of PSNR values for despeckled results using synthetic noise on Fig. 2(a) at different noise levels.

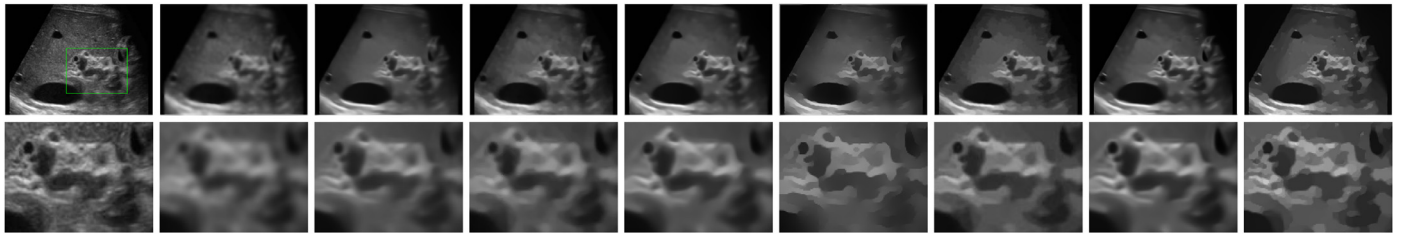
	$\sigma^2 = 0.2$	$\sigma^2 = 0.25$	$\sigma^2 = 0.3$	$\sigma^2 = 0.35$
SRAD	21.34	20.10	19.18	18.42
OBFLM	18.97	18.34	17.77	17.34
ADLG	20.83	19.74	18.88	18.17
NLMLS	23.38	22.35	21.68	20.97
FPC	22.30	21.21	20.33	19.46
BNLTv	25.85	24.40	23.43	22.52
LDCNN	24.62	23.40	22.51	21.76
Ours	26.87	25.90	24.72	23.91

method on another four noise levels $\sigma^2 = \{0.2, 0.25, 0.3, 0.35\}$ on the same clean image (see Fig. 2(a)), and compare despeckled results of different methods. Table 2 summaries the resulting PSNR values over all the methods, indicating that our method consistently has better performance over others.

4.2. Clinical images

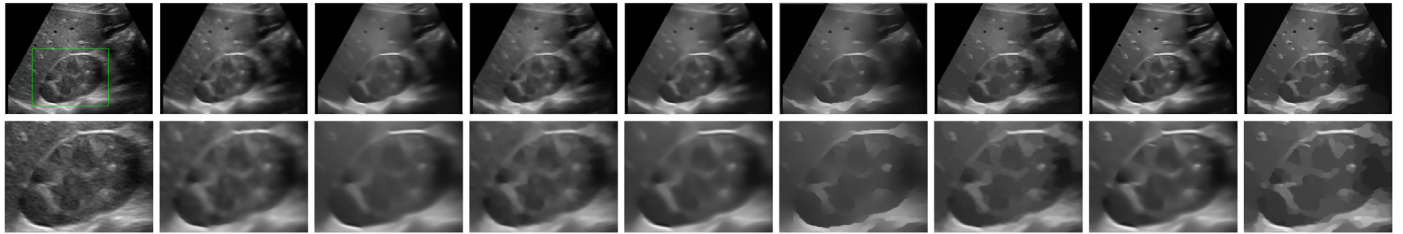
We further verify the proposed method on many clinical images obtained from a public ultrasound dataset¹. Compared to the conference version [23], more new clinical images are included for comparisons to further verify the effectiveness of the proposed method. We show the results of six typical images from Figs. 5 to 10 and more results can be found in the supplementary material. Figs. 5–Fig. 7 demonstrate the despeckling results of three different ultrasound images. As shown in those blown-up views, our method effectively removes speckle noise while clearly preserving boundaries of the main tissues and small regions, but other methods heavily blur those boundaries and even smooth out edges of small regions. Moreover, despeckling results of another three ultrasound images are shown in Figs. 8–10, in which the top row illustrates despeckled results while the bottom row shows the intensity profiles of a typical vertical or horizontal line. The despeckling results visually demonstrate the proposed L_0 minimization achieves best performance in maintaining features of the input ultrasound images among all the compared despeckling techniques. The intensity profiles further demonstrate that our method does not alter peak values of prominent features in the original image, while suppressing intensity fluctuates caused by

¹ <http://www.ultrasoundcases.info>



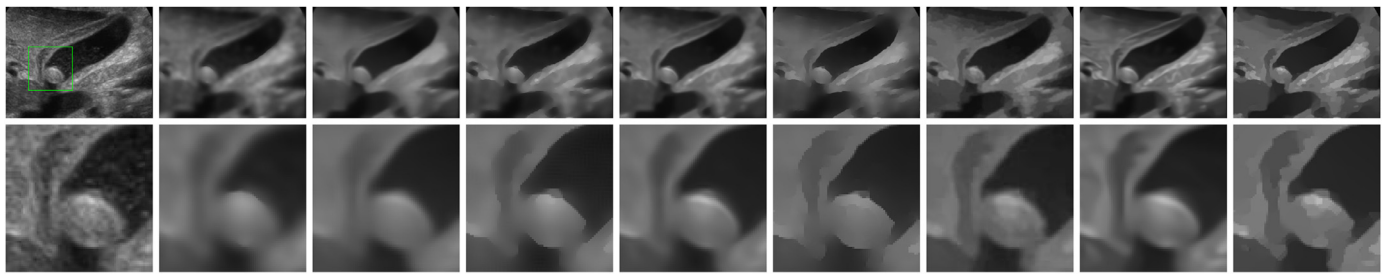
(a) Input (b) SRAD [19] (c) OBFLM [7] (d) ADLG [2] (e) NLMLS [8] (f) FPC [14] (g) BNLTv [20] (h) LDCNN [21] (i) Our method

Fig. 5. Comparison of speckle reduction on an ultrasound image. (a) Original image. Despeckled result by (b) SRAD [19], (c) OBFLM [7], (d) ADLG [2], (e) NLMLS [8], (f) FPC [14], (g) BNLTv [20], (h) LDCNN [21], and (i) our method.



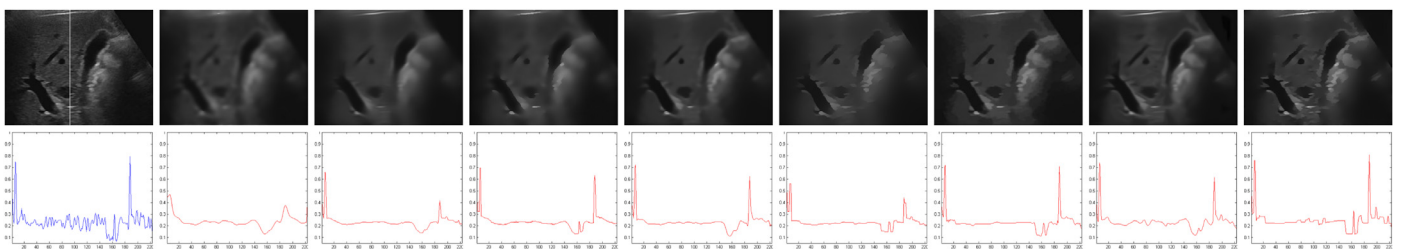
(a) Input (b) SRAD [19] (c) OBFLM [7] (d) ADLG [2] (e) NLMLS [8] (f) FPC [14] (g) BNLTv [20] (h) LDCNN [21] (i) Our method

Fig. 6. Comparison of speckle reduction on an ultrasound image. (a) Original image. Despeckled result by (b) SRAD [19], (c) OBFLM [7], (d) ADLG [2], (e) NLMLS [8], (f) FPC [14], (g) BNLTv [20], (h) LDCNN [21], and (i) our method.



(a) Input (b) SRAD [19] (c) OBFLM [7] (d) ADLG [2] (e) NLMLS [8] (f) FPC [14] (g) BNLTv [20] (h) LDCNN [21] (i) Our method

Fig. 7. Comparison of speckle reduction on an ultrasound image with a mobile gallstone. (a) Original image. Despeckled result by (b) SRAD [19], (c) OBFLM [7], (d) ADLG [2], (e) NLMLS [8], (f) FPC [14], (g) BNLTv [20], (h) LDCNN [21], and (i) our method.



(a) Input (b) SRAD [19] (c) OBFLM [7] (d) ADLG [2] (e) NLMLS [8] (f) FPC [14] (g) BNLTv [20] (h) LDCNN [21] (i) Our method

Fig. 8. Comparison of speckle reduction on a hypoechoic liver ultrasound image with metastatic melanoma, as well as the evaluation of the feature contrast preservation. (a) Original image with the intensity profile (blue curve) of a vertical line. Despeckled result with its intensity profile (red curve) by (b) SRAD [19], (c) OBFLM [7], (d) ADLG [2], (e) NLMLS [8], (f) FPC [14], (g) BNLTv [20], (h) LDCNN [21], and (i) our method (For interpretation of the references to color in this figure legend, the reader is referred to the web version of this article.).

speckle noise. In contrast, other methods are all obviously reduce peak values of those features to some extent.

Fig. 11 presents our despeckling results on more clinical images. From the results, we can observe that our method can effectively remove speckle noise and maintain features at the same time. In addition, many originally blurry features are much clearer in our despeckled results. We also invite some clinical experts to comment on our results, and they conclude that our results of speckle reduction improve the image quality and well protect

the structure details, which can provide helps for their clinical computer-aided diagnosis systems.

4.3. Effects of parameters

As discussed in the second paragraph of the Section 4, Our method has two parameters to be turned for different input ultrasound images: k and λ . k controls the increasing speed starting from β_0 to β_{\max} , and thus more iterations are required in our

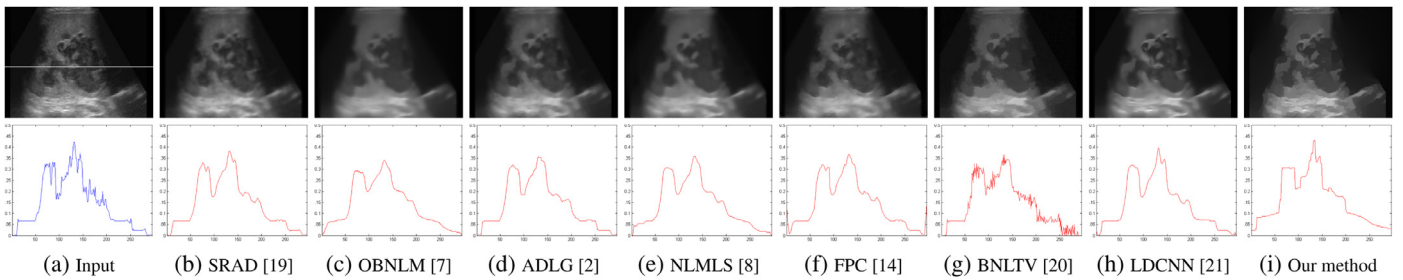


Fig. 9. Comparison of speckle reduction on an ultrasound image, as well as the evaluation of the feature contrast preservation. (a) Original image with the intensity profile (blue curve) of a vertical line. Despeckled result with its intensity profile (red curve) by (b) SRAD [19], (c) OBNLM [7], (d) ADLG [2], (e) NLMLS [8], (f) FPC [14], (g) BNLTV [20], (h) LDCNN [21], and (i) our method. By observing the intensity profiles of the vertical line, we can find that our method has superior performance of maintaining feature intensity contrasts (For interpretation of the references to color in this figure legend, the reader is referred to the web version of this article.)

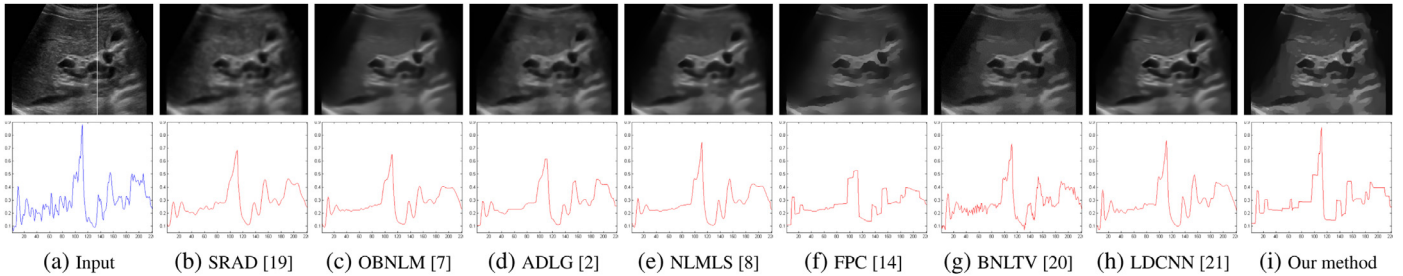


Fig. 10. Comparison of speckle reduction on an ultrasound image, as well as the evaluation of the feature contrast preservation. (a) Original image with the intensity profile (blue curve) of a vertical line. Despeckled result with its intensity profile (red curve) by (b) SRAD [19], (c) OBNLM [7], (d) ADLG [2], (e) NLMLS [8], (f) FPC [14], (g) BNLTV [20], (h) LDCNN [21], and (i) our method. By observing the intensity profiles of the vertical line, we can find that our method has superior performance of maintaining feature intensity contrasts (For interpretation of the references to color in this figure legend, the reader is referred to the web version of this article.)

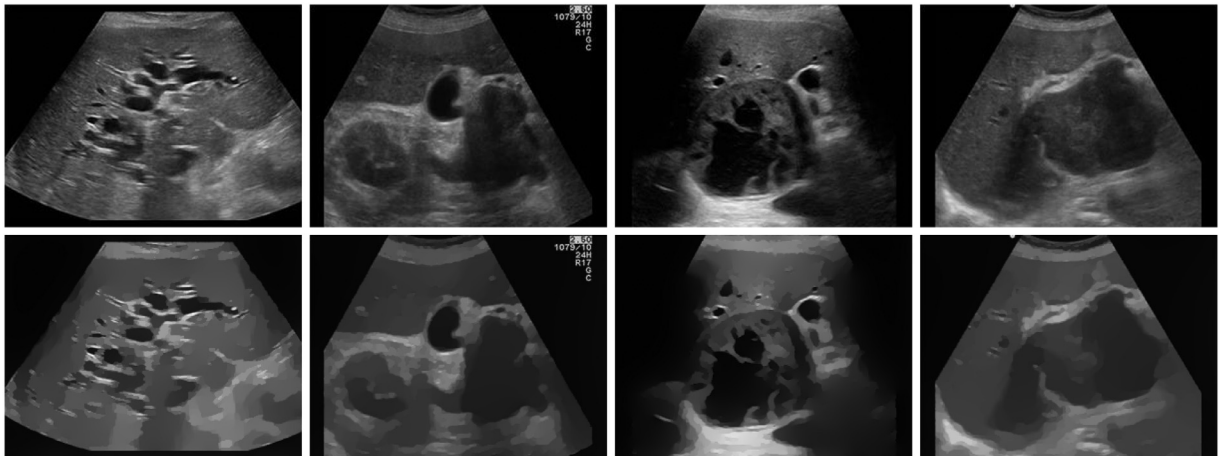


Fig. 11. More despeckled results produced by our method. Top row: inputs. Bottom row: our results. It is observed that our method can consistently maintain features in the inputs of different tissue regions and effectively remove speckle noise.

optimization for a smaller k . However, the results of the proposed methods are not that sensitive to the change of k . A small k tends to blur some edges during exceeding iterations, while a large k may preserve some noise around edges, due to a fast optimization process in our method. In Fig. 12, we show the effect of changing k on the despeckled result of an synthetic image (see Fig. 12 (b)). When taking a closer look at the results, we can notice tiny changes cause by the adjustment of k , which is also proved by the PSNR values for different despeckled results.

On the other hand, the critical parameter λ is allowed to be adjusted to decide the speckle noise removal ability of our method. While a small λ is insufficient to remove the most of speckle noise, a large λ tend to more blur some features. Fig. 13 presents the effect of changing λ on the despeckled result of Fig. 12 (b). It is observed that when λ is small, the despeckled result is not

satisfactory. With the increase of λ , the speckle reduction ability of our method is enhanced accompanying by blurring of some features, leading to a smaller PSNR values (see Fig. 12 (j)). With a proper λ , our method can effectively eliminate speckle noise and preserve features at the same time.

4.4. Application to ultrasound image segmentation

Afterwards, we demonstrate the proposed method can be employed as a prerequisite step in intelligent ultrasound processing systems by taking the image segmentation as an example. Breast tumor segmentation plays a vital role in the computer-aided diagnosis (CAD) system, since the clinical benign and malignant breast lesion classification relies on the shape or contour features from segmented lesions [2]. In Fig. 14, we present the segmentation

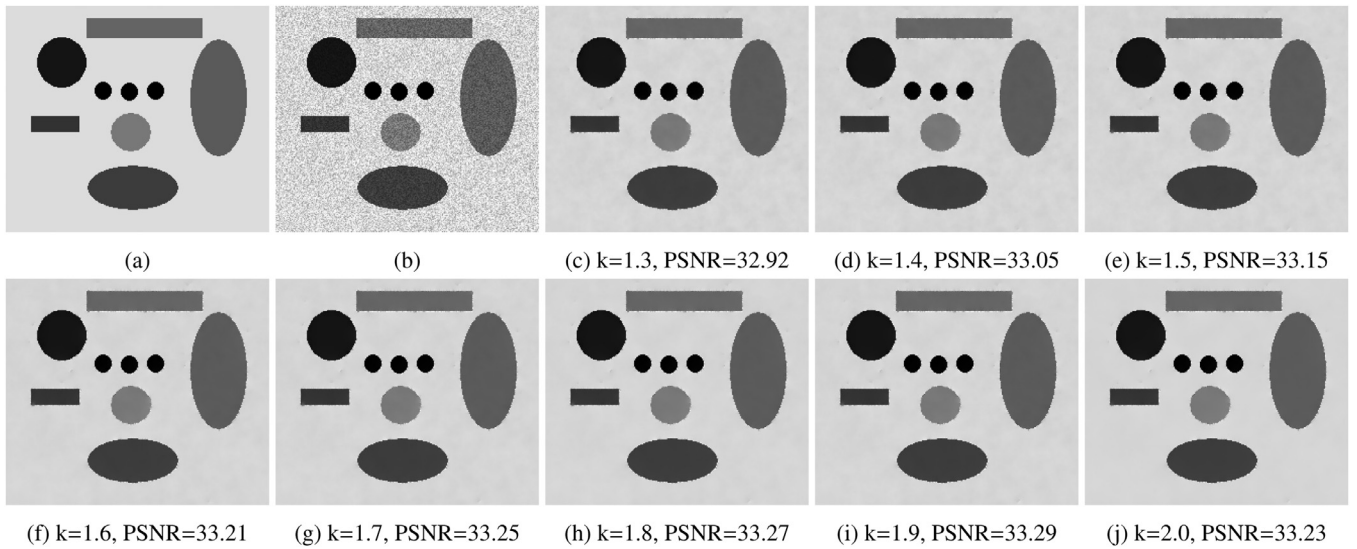


Fig. 12. Effect of parameters k . (a) Clean image. (b) synthetic image. (c)-(j) show the despeckled results by tuning k and the corresponding PSNR value.

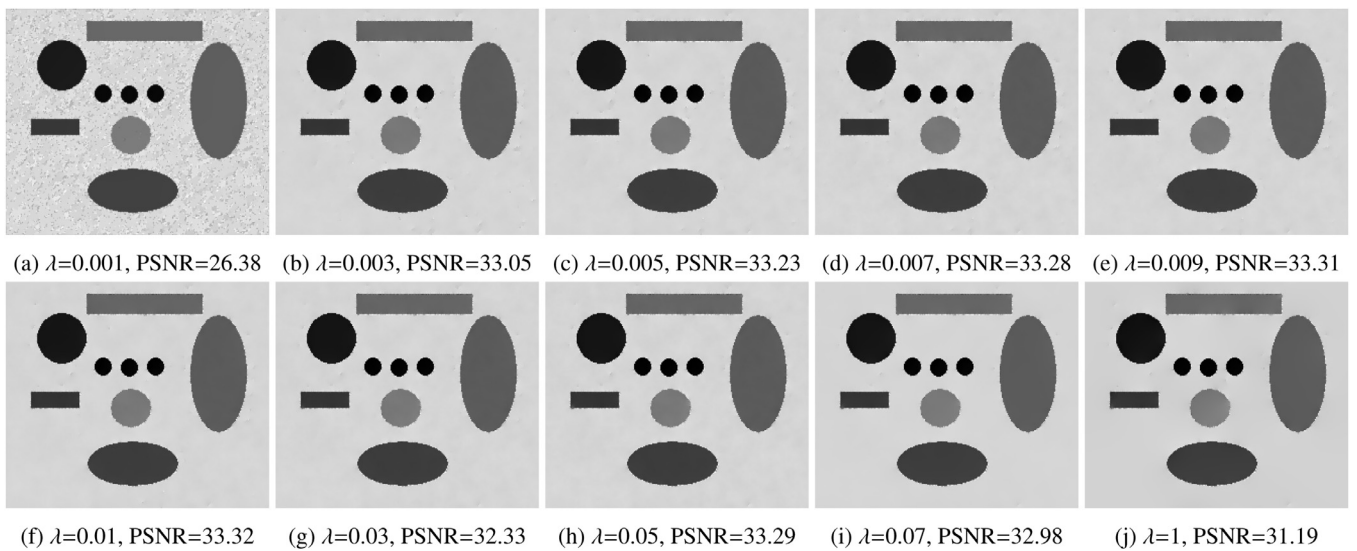


Fig. 13. Effect of parameters λ . (a) Clean image. (b) synthetic image. (c)-(j) show the despeckled results with different λ values and the corresponding PSNR value.

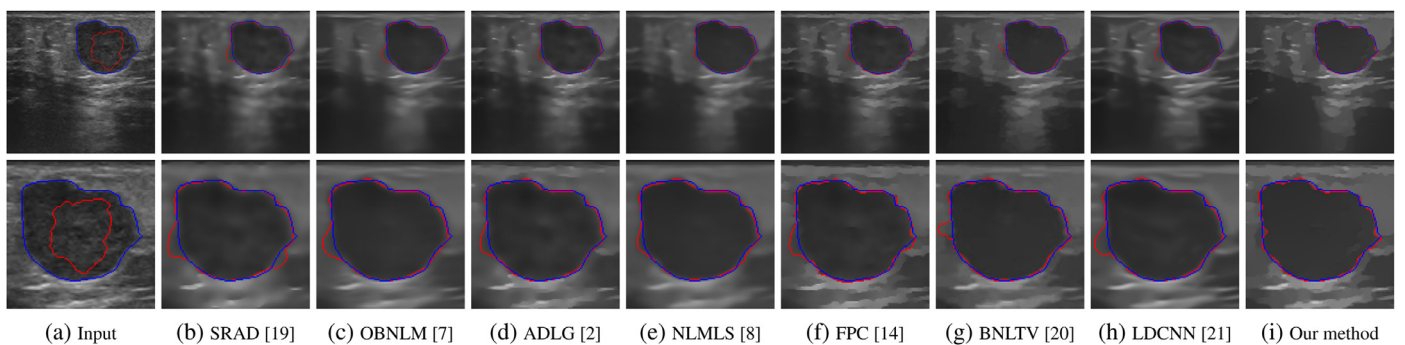


Fig. 14. Breast tumor segmentation accuracy comparison on different despeckled results. (a) The original ultrasound image and its segmentation result. Despeckled result and its segmentation result by (b) SRAD [19], (c) OBFLM [7], (d) ADLG [2], (e) NLMLS [8], (f) FPC [14], (g) BNLTV [20], (h) LDCNN [21], and (i) our method. Blue color: the ground truth delineated by clinicians; Red color: the reached segmentation result (For interpretation of the references to color in this figure legend, the reader is referred to the web version of this article.)

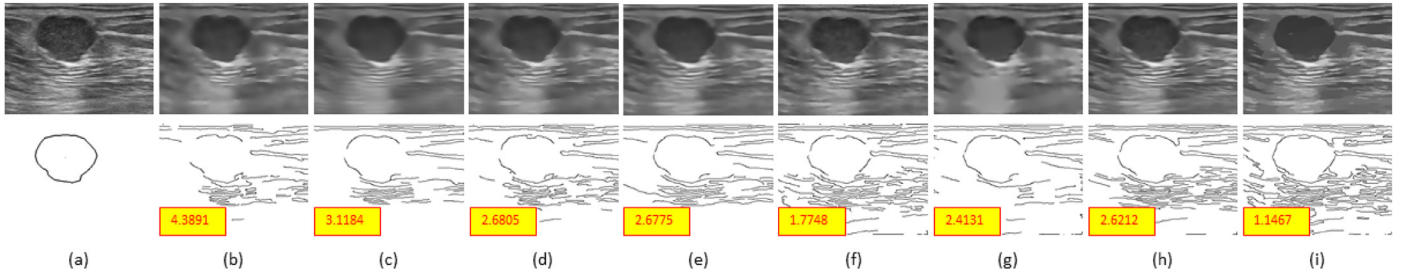


Fig. 15. Evaluation of the lesion boundary preservation in despeckled results of an input ultrasound image with a lesion in the right breast. (a) the original ultrasound image, and the breast lesion boundary delineated by the clinical doctor; The despeckled result by (b) SRAD [19], (c) OBNLM [7], (d) ADLG [2], (e) NLMLS [8], (f) FPC [14], (g)BNLTV [20], (h) LDCNN [21], and (i) our method, and the edge maps (with MRD value) obtained by running the Canny's detector. In edge maps of (b)–(i), rectangles at the bottom-left corner show the corresponding mean radial distance (MRD) results produced from different despeckled results.

Table 3

Mean AC, HD and HM values for different segmentation results on 10 ultrasound images.

	Input	SRAD	OBNLM	ADLG	NLMLS	FPC	BNLTV	LDCNN	Ours
AC (%)	63.46	91.00	93.44	94.03	94.25	94.47	95.48	96.18	97.71
HD	30.4451	10.8214	6.5745	4.4619	5.1225	7.8611	11.2947	11.2403	2.8892
HM	12.785	2.4559	1.8404	1.7014	1.5687	1.3979	1.1842	1.4421	0.6356

Table 4

Median AC, HD and HM values for different segmentation results on 10 ultrasound images.

	Input	SRAD	OBNLM	ADLG	NLMLS	FPC	BNLTV	LDCNN	Ours
AC (%)	72.97	94.29	94.85	95.66	95.67	95.47	96.18	95.02	97.75
HD	37.5402	10.9965	8.3353	8.0297	7.5421	6.9182	6.3796	9.37	2.7319
HM	11.6133	2.116	1.9286	1.5741	1.5771	1.6422	1.3955	1.8183	0.8835

results of the breast tumor on the speckled image and despeckled images by employing a famous level set based segmentation technique [26]. The red curve is the obtained segmentation result and the blue curve is the manual result delineated by a clinical doctor, which is usually regarded as the ground truth [42]. As can be seen, the segmentation performance on the original image is pretty poor, due to the adverse effect from the speckle noise. Carrying out the segmentation on those despeckled image, we find that the accuracy has been significantly improved. Among all despeckled images, the segmentation result on our despeckled result is closest to the ground truth. Since some parts of the breast tumor contour are blurred in other despeckled results, their segmentation contours leaks out the blurred edges.

In addition, three metrics [26]: a combined accuracy metric of true and false positive rate (AC), Hausdorff distance (HD) and Hausdorff mean (HM), are adopted for quantitative comparison. The region based metric AC evaluates the segmentation accuracy by measuring the overlapping rate of manual and obtained segmentation regions, while HD and HM computes the distance of the boundaries between the manual and obtained segmentation results. Hence, a better segmentation result shall have higher AC, as well as lower HD and HM. Table 3 summaries mean values of three metrics for different segmentation results of 10 ultrasound images. Obviously, our result achieves the largest AC value (97.71%), the smallest HD value (2.8892) and the smallest HM value (0.6356) among all despeckled results. Moreover, we report the median three metric values for 10 segmentation results on despeckled results produced by different methods in Table 4. From the results, we can easily observe that segmentations on our despeckled results also achieve best results among all the segmentation results.

4.5. Application to lesion boundary preservation

Breast ultrasound (BUS) is a vital adjunct of the mammography for patients with palpable mass or inconclusive mammograms. Computer-aided diagnosis systems usually extract the shape or

contour of the breast lesions to identify them as benign or malignant in BUS images [4], but the speckle noise in BUS images complicates this task. When applying a despeckling procedure as a pre-processing step, we can easily pick up the lesion boundary, due to the removal of speckle noise, and the performance thus depends on the lesion boundary preservation of the despeckling technique. To quantitatively evaluate the edge preservation in clinical ultrasound images, we use the mean radial distance (MRD) metric [2], and compare their values of different techniques to further verify the effectiveness of our method. Let E_1 denotes the set of points on the breast lesion boundary delineated by the clinical doctor, and E_2 represents the obtained edge map by the Canny detector. Then, MRD is defined as:

$$MRD = \frac{1}{\tau} \sum_{p_i \in E_1} \|p_i - r_j\|, \quad (20)$$

where r_j is the point in the E_2 , which has the minimum distance to p_i in the same radial direction from the lesion centroid, and thus the smaller MRD value implies that the despeckling method has a better edge preservation after speckle reduction.

In the top row of Fig. 15, we compare the despeckled result of a breast ultrasound image. As can be seen, our method can efficiently suppress the speckle noise and best preserve the breast lesion, but the price paid for removing speckle noise is the blurring of the lesion in other despeckling techniques. Moreover, we employ the MRD to quantitatively evaluate the boundary preservation of the breast lesion, and the MRD value is presented in the bottom-left rectangle of Fig. 15. Obviously, our method reaches the smallest MRD value with 1.1467 pixels, which indicates that the despeckled image by our method best preserves the breast lesion's boundary among all despeckled resultant images.

5. Conclusion

We presented a novel L_0 minimization framework tailored for speckle reduction in ultrasound images. First, we formulated a

sparse prior of a new measure *GAP*, which takes both the gradient and phase information into consideration. With the prior, we proposed a global minimization to seek for the L_0 sparsity of the *GAP*. In addition, we proposed an efficient and robust solver, which transfers the intractable L_0 minimization into several optimization steps with closed-form solutions. Experiments in synthetic and clinical ultrasound images demonstrate that our approach outperforms state-of-the-art methods for speckle reduction. The proposed method has great potential to be applied to many intelligent ultrasound systems. In the future, we will accelerate our L_0 minimization using GPU, and also test our despeckling method on more clinical ultrasound images and applications.

Acknowledgments

The work presented in this paper was supported by a grant from Shenzhen Science and Technology Program (No.JCYJ20160429190300857), a grant from Shenzhen Science and Technology Program (JCYJ20170413162617606), a grant from Shenzhen Science and Technology Program (No.JCYJ20150925163244742), a grant from Gongdong Natural Science Foundation Project (Project no. 2016A030313047), a grant from the science and technology plan project of guangzhou (No.201704020141), a grant from Guangdong province science and technology plan project (No.2016A020220013), a grant from the Hong Kong Research Grants Council (No. PolyU 152040/16E), and a grant from the Innovation and Technology Fund of Hong Kong (Project no. ITS/304/16).

Appendix A

Here, we prove that the closed-form solution of Eq. (14) is achieved under the condition in Eq. (15). To simplify the expression, we introduce J_q to denote the energy function at the particular pixel q in Eq. (14):

$$J_q = (\partial_x D_q - u_q)^2 + (\partial_y D_q - v_q)^2 + (FA(D)_q - w_q)^2 + \frac{\lambda}{\beta} R(u_q^2 + v_q^2 + w_q^2). \quad (\text{A.1})$$

If $(u_q, v_q, w_q) = (0, 0, 0)$, $R(u_q^2 + v_q^2 + w_q^2) = 0$. Then, J_q becomes:

$$J_q = (\partial_x D_q - 0)^2 + (\partial_y D_q - 0)^2 + (FA(D)_q - 0)^2 = \partial_x D_q^2 + \partial_y D_q^2 + FA(D)_q^2 = GAP(D)_q. \quad (\text{A.2})$$

Otherwise, $R(u_q^2 + v_q^2 + w_q^2) = 1$, so that J_q can be computed as:

$$J_q = (\partial_x D_q - u_q)^2 + (\partial_y D_q - v_q)^2 + (FA(D)_q - w_q)^2 + \frac{\lambda}{\beta}. \quad (\text{A.3})$$

Hence, when $(u_q, v_q, w_q) = (\partial_x D_q, \partial_y D_q, FA(D)_q)$, J_p reaches the minimal value $\frac{\lambda}{\beta}$.

By comparing the minimal values of Eq. (A.2) and Eq. (A.3), we discuss the optimization of J_q in the following two conditions:

Case 1: $GAP(D)_q < \frac{\lambda}{\beta}$. J_q achieves the minimum value $(GAP(D)_q)$ under the condition $(u_q, v_q, w_q) = (0, 0, 0)$.

Case 2: $GAP(D)_q \geq \frac{\lambda}{\beta}$. when $(u_q, v_q, w_q) = (\partial_x D_q, \partial_y D_q, FA(D)_q)$, J_q achieves the minimal value $\frac{\lambda}{\beta}$.

Hence, J_q reaches the closed-form solution under the following condition:

$$(u_q, v_q, w_q) = \begin{cases} (\partial_x D_q, \partial_y D_q, FA(D)_q), & GAP(D)_q > \frac{\lambda}{\beta} \\ (0, 0, 0), & \text{otherwise.} \end{cases} \quad (\text{A.4})$$

Supplementary material

Supplementary material associated with this article can be found, in the online version, at [10.1016/j.neucom.2018.03.009](https://doi.org/10.1016/j.neucom.2018.03.009)

References

- [1] G. Vegas-Sanchez-Ferrero, S. Aja-Fernandez, M. Martín-Fernández, A.F. Frangi, C. Palencia, Probabilistic-driven oriented speckle reducing anisotropic diffusion with application to cardiac ultrasonic images, in: International Conference On Medical Image Computing and Computer Assisted Intervention, Springer, 2010, pp. 518–525.
- [2] W.G. Flores, W.C. de Albuquerque Pereira, A.F.C. Infantosi, Breast ultrasound despeckling using anisotropic diffusion guided by texture descriptors, *Ultrasound Med. Biol.* 40 (11) (2014) 2609–2621.
- [3] B. Wang, T. Cao, Y. Dai, D.C. Liu, Ultrasound speckle reduction via super resolution and nonlinear diffusion, in: Proceedings of the Asian Conference on Computer Vision, Springer, 2009, pp. 130–139.
- [4] H. Cheng, J. Shan, W. Ju, Y. Guo, L. Zhang, Automated breast cancer detection and classification using ultrasound images: a survey, *Pattern Recognit.* 43 (1) (2010) 299–317.
- [5] S. Esakkirajan, C.T. Vimalraj, R. Muhammed, G. Subramanian, Adaptive wavelet packet-based de-speckling of ultrasound images with bilateral filter, *Ultrasound Med. Biol.* 39 (12) (2013) 2463–2476.
- [6] S. Balocco, C. Gatta, O. Pujol, J. Mauri, P. Radeva, Srbf: speckle reducing bilateral filtering, *Ultrasound Med. Biol.* 36 (8) (2010) 1353–1363.
- [7] P. Coupé, P. Hellier, C. Kervrann, C. Barillot, Nonlocal means-based speckle filtering for ultrasound images, *IEEE Trans. Image Process.* 18 (10) (2009) 2221–2229.
- [8] J. Yang, J. Fan, D. Ai, X. Wang, Y. Zheng, S. Tang, Y. Wang, Local statistics and non-local mean filter for speckle noise reduction in medical ultrasound image, *Neurocomputing* 195 (2016) 88–95.
- [9] P.C. Tay, C.D. Garson, S.T. Acton, J.A. Hossack, Ultrasound despeckling for contrast enhancement, *IEEE Trans. Image Process.* 19 (7) (2010) 1847–1860.
- [10] D. Min, S. Choi, J. Lu, B. Ham, K. Sohn, M.N. Do, Fast global image smoothing based on weighted least squares, *IEEE Trans. Image Process.* 23 (12) (2014) 5638–5653.
- [11] L. Xu, C. Lu, Y. Xu, J. Jia, Image smoothing via l_0 gradient minimization, *ACM Trans. Graph.* 30 (6) (2011) 174.
- [12] Z. Li, J. Zheng, Z. Zhu, W. Yao, S. Wu, Weighted guided image filtering, *IEEE Trans. Image Process.* 24 (1) (2015) 120–129.
- [13] Z. Farbman, R. Fattal, D. Lischinski, R. Szeliski, Edge-preserving decompositions for multi-scale tone and detail manipulation, *ACM Trans. Graph.* 27 (3) (2008).
- [14] L. Zhu, W. Wang, J. Qin, K.-H. Wong, K.-S. Choi, P.-A. Heng, Fast feature-preserving speckle reduction for ultrasound images via phase congruency, *Signal Process.* 134 (2017) 275–284.
- [15] L. Xu, S. Zheng, J. Jia, Unnatural l_0 sparse representation for natural image deblurring, in: Proceedings of the IEEE Conference on Computer Vision and Pattern Recognition, 2013, pp. 1107–1114.
- [16] J. Pan, Z. Hu, Z. Su, M.-H. Yang, Deblurring text images via l_0 -regularized intensity and gradient prior, in: Proceedings of the IEEE Conference on Computer Vision and Pattern Recognition, IEEE, 2014, pp. 2901–2908.
- [17] S. Yi, X. Wang, C. Lu, J. Jia, L_0 regularized stationary time estimation for crowd group analysis, in: Proceedings of the IEEE Conference on Computer Vision and Pattern Recognition, 2014, pp. 2211–2218.
- [18] J. Yu, J. Tan, Y. Wang, Ultrasound speckle reduction by a susan-controlled anisotropic diffusion method, *Pattern Recognit.* 43 (9) (2010) 3083–3092.
- [19] Y. Yu, S.T. Acton, Speckle reducing anisotropic diffusion, *IEEE Trans. Image Process.* 11 (11) (2002) 1260–1270.
- [20] T. Wen, J. Gu, L. Li, W. Qin, L. Wang, Y. Xie, Nonlocal total-variation-based speckle filtering for ultrasound images, *Ultrasound Imaging* 38 (4) (2016) 254–275.
- [21] K. Zhang, W. Zuo, S. Gu, L. Zhang, Learning deep CNN denoiser prior for image restoration, in: Proceedings of the Conference on Computer Vision and Pattern Recognition (2017).
- [22] A. Belaïd, D. Boukerrouy, Y. Maingourd, J.-F. Lerallut, Phase-based level set segmentation of ultrasound images, *IEEE Trans. Inf. Technol. Biomed.* 15 (1) (2011) 138–147.
- [23] L. Zhu, W. Wang, X. Li, Q. Wang, J. Qin, K.-H. Wong, P.-A. Heng, Ultrasound speckle reduction via l_0 minimization, in: Proceedings of the Asian Conference on Computer Vision, Springer, 2016.
- [24] A. Khare, M. Khare, Y. Jeong, H. Kim, M. Jeon, Despeckling of medical ultrasound images using Daubechies complex wavelet transform, *Signal Process.* 90 (2) (2010) 428–439.
- [25] P. Perona, J. Malik, Scale-space and edge detection using anisotropic diffusion, *IEEE Trans. Pattern Anal. Mach. Intell.* 12 (7) (1990) 629–639.
- [26] F.M. Cardoso, M.M. Matsumoto, S.S. Furuie, Edge-preserving speckle texture removal by interference-based speckle filtering followed by anisotropic diffusion, *Ultrasound Med. Biol.* 38 (8) (2012) 1414–1428.
- [27] F. Zhang, Y.M. Yoo, K.L. Mong, Y. Kim, Nonlinear diffusion in Laplacian pyramid domain for ultrasonic speckle reduction, *IEEE Trans. Med. Imaging* 26 (2) (2007) 200–211.
- [28] D.T. Kuan, A.A. Sawchuk, T.C. Strand, P. Chavel, Adaptive noise smoothing filter for images with signal-dependent noise, *IEEE Trans. Pattern Anal. Mach. Intell.* 7 (2) (1985) 165–177.

- [29] A. Buades, B. Coll, J.-M. Morel, A non-local algorithm for image denoising, in: Proceedings of the Conference on Computer Vision and Pattern Recognition, 2005, pp. 60–65.
- [30] B. Du, W. Xiong, J. Wu, L. Zhang, L. Zhang, D. Tao, Stacked convolutional denoising auto-encoders for feature representation, *IEEE Trans. Cybern.* 47 (4) (2017) 1017–1027.
- [31] M.C. Morrone, J. Ross, D.C. Burr, R. Owens, Mach bands are phase dependent, *Nature* 324 (6094) (1986) 250–253.
- [32] P. Kovessi, Symmetry and asymmetry from local phase, in: Proceedings of the Tenth Australian Joint Conference on Artificial Intelligence, 190, Citeseer, 1997.
- [33] P. Kovessi, Image features from phase congruency, *Videre J. Comput. Vis. Res.* 1 (3) (1999) 1–26.
- [34] D. Boukerroui, J.A. Noble, M. Brady, On the choice of band-pass quadrature filters, *J. Math. Imaging Vis.* 21 (1–2) (2004) 53–80.
- [35] T. Lindeberg, Edge detection and ridge detection with automatic scale selection, *Int. J. Comput. Vis.* 30 (2) (1998) 117–156.
- [36] D. Geman, C. Yang, Nonlinear image recovery with half-quadratic regularization, *IEEE Trans. Image Process.* 4 (7) (1995) 932–946.
- [37] D. Krishnan, R. Fergus, Fast image deconvolution using hyper-Laplacian priors, in: Proceedings of the Advances in Neural Information Processing Systems, 2009, pp. 1033–1041.
- [38] I. Daubechies, R. DeVore, M. Fornasier, C.S. Güntürk, Iteratively reweighted least squares minimization for sparse recovery, *Commun. Pure Appl. Math.* 63 (1) (2010) 1–38.
- [39] L. Xu, Q. Yan, Y. Xia, J. Jia, Structure extraction from texture via relative total variation, *ACM Trans. Graph.* 31 (6) (2012) 139.
- [40] J. Zhang, G. Lin, L. Wu, Y. Cheng, Speckle filtering of medical ultrasonic images using wavelet and guided filter, *Ultrasonics* 65 (2016) 177–193.
- [41] Z. Wang, A.C. Bovik, H.R. Sheikh, E.P. Simoncelli, Image quality assessment: from error visibility to structural similarity, *IEEE Trans. Image Process.* 13 (4) (2004) 600–612.
- [42] L. Massoptier, S. Casciari, A new fully automatic and robust algorithm for fast segmentation of liver tissue and tumors from ct scans, *Eur. Radiol.* 18 (8) (2008) 1658–1665.



Lei Zhu is a postdoctoral fellow in the Hong Kong Polytechnic University. He received a Ph.D. in Computer Science and Engineering, the Chinese University of Hong Kong. His research interests focus on computer graphics, computer vision, and medical imaging.



Weiming Wang received his Ph.D. degree in computer science and engineering from The Chinese University of Hong Kong, and B.S. degree from Huazhong University of Science and Technology. His research interests include medical image processing, rendering and visualisation, virtual reality, and medical robotics.



Xiaomeng Li received the bachelor degree in college of electromechanical engineering from XiDian University, China, and is currently pursuing the doctor degree in computer science and engineering in The Chinese University of Hong Kong. Her current research interests include object segmentation, medical image analysis and deep learning.



Qiong Wang received her Ph.D. degree in Computer Science and Engineering at the Chinese University of Hong Kong, Hong Kong. She is currently an Assistant Professor in Shenzhen Institutes of Advanced Technology, Chinese Academy of Sciences. Her research interests include human-computer interaction, haptics, virtual reality, and computer-assisted surgery.



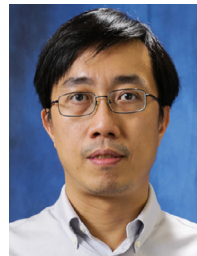
Jing Qin is an assistant professor in School of Nursing, The Hong Kong Polytechnic University. He is also a key member in the Centre for Smart Health, SN, PolyU, HK. He received his Ph.D. degree in Computer Science and Engineering from the Chinese University of Hong Kong in 2009. Dr. Qins research interests include innovations for healthcare and medicine applications, medical image processing, deep learning, visualization and human-computer interaction and health informatics.



Kin-Hong Wong is an Associate Professor of the Department of Computer Science and Engineering of the Chinese University of Hong Kong. He received a Ph.D. from the Department of Engineering of the University of Cambridge. His major research interest is in 3-D computer vision especially in pose estimation, structure from motion and tracking. He has investigated and developed many useful techniques in computer vision such as the four-point pose estimation algorithm and Kalman-trifocal pose estimation methods which are useful in many application areas such as automatic driving and virtual reality. He is also interested in pattern recognition, embedded applications, and computer music.



Kup-Sze Choi received his Ph.D. degree in computer science and engineering from the Chinese University of Hong Kong. He is currently an associate professor at the School of Nursing of the Hong Kong Polytechnic University, and the Director of the Centre for Smart Health and the PolyU-Henry G. Leong Mobile Integrative Health Centre. His research interests are healthcare innovations, with focus on virtual reality and artificial intelligence applications.



Chi-Wing Fu joined the Chinese University of Hong Kong as an associate professor in 2016. He obtained his Ph.D. in Computer Science from Indiana University Bloomington, USA. He served as program co-chair of SIGGRAPH ASIA 2016 technical brief and poster programs, associate editor of Computer Graphics Forum, as well as TPC members in various conferences and technical programs, such as SIGGRAPH ASIA technical brief, emerging technology, IEEE Visualization (SciVis), and ACM CHI Work-in-Progress. His research interests include computer graphics, visualization, and user interaction research in HCI.



Pheng-Ann Heng received the Ph.D. degree in computer science from Indiana University Bloomington in 1992. He is a professor at the Chinese University of Hong Kong Department of Computer Science and Engineering. His research interests include VR applications in medicine, visualization, medical imaging, human-computer interaction, and computer graphics. He is a senior member of the IEEE.